Carbohydrate Polymers 90 (2012) 1244–1253

Contents lists available at SciVerse ScienceDirect

Carbohydrate Polymers

journal homepage: www.elsevier.com/locate/carbpol

Preparation and evaluation of warfarin-β-cyclodextrin loaded chitosan nanoparticles for transdermal delivery

Safaa K.H. Khalil[a,*], Gina S. El-Feky[b], Sally T. El-Banna[a], Wafaa A. Khalil[c]

[a] Advanced Materials and Nanotechnology Group, Center of Excellence for Advanced Sciences (CEAS), Department of Spectroscopy, Division of Physics, National Research Center, Cairo, Egypt
[b] Department of Pharmaceutical Technology, Division of Pharmaceutics, National Research Center, Cairo, Egypt
[c] Depatment of Biophysics, Faculty of Science, University of Cairo, Cairo, Egypt

ARTICLE INFO

Article history:
Received 23 February 2012
Received in revised form 19 May 2012
Accepted 21 June 2012
Available online 29 June 2012

Keywords:
Chitosan
Cyclodextrin
Nanoparticles
Transdermal
Warfarin

ABSTRACT

The main objective of the present work was to prepare warfarin-β-cyclodextrin (WAF-β-CD) loaded chitosan (CS) nanoparticles for transdermal delivery. CS is a hydrophilic carrier therefore, to overcome the hydrophobic nature of WAF and allow its incorporation into CS nanoparticles, WAF was first complexed with β-cyclodextrin (β-CD). CS nanoparticles were prepared by ionotropic pre-gelation using tripolyphosphate (TPP). Morphology, size and structure characterization of nanoparticles were carried out using SEM, TEM and FTIR, respectively. Nanoparticles prepared with 3:1 CS:TPP weight ratio and 2 mg/ml final CS concentration were found optimum. They possessed spherical particles (35 ± 12 nm diameter) with narrow size distribution (PDI = 0.364) and 94% entrapment efficiency. The *in vitro* release as well as the *ex vivo* permeation profiles of WAF-β-CD from the selected nanoparticle formulation were studied at different time intervals up to 8 h. *In vitro* release of WAF-β-CD from CS nanoparticles followed a Higuchi release profile whereas its *ex vivo* permeation (at pH 7.4) followed a zero order permeation profile. Results suggested that the developed WAF-β-CD loaded CS carrier could offer a controlled and constant delivery of WAF transdermally.

1. Introduction

Considerable research is being directed towards developing polymeric nanoparticles for drug delivery (Panyam & Labhasetwar, 2003; Shenoy & Amiji, 2005). Among water-soluble polymers used, CS is the most extensively studied (Morishita & Peppas, 2006; Wilson et al., 2009) due to the ideal properties it possesses such as biocompatibility, biodegradability, low cost, positive charge and absorption enhancing effect (De Campos, Sanchez, & Alonso, 2001; Illum, Jabbal-Gill, Hinchcliffe, Fisher, & Davis, 2001; Muzzrelli, 2012). In addition to the great interest CS has received recently as transdermal drug carrier due to its bioadhesion, permeability-enhancing properties and interesting physico-chemical characteristics (Langoth et al., 2006; Mei, Mao, Sun, Wang, & Kissel, 2008; Ozcan et al., 2009). However, its hydrophilic nature has limited its use to delivering hydrophilic drugs. Currently, new nanocarriers of CS/CD were synthesized; the novel nanoparticles could encapsulate hydrophobic drugs successfully by introducing CDs (Grenha et al., 2008; Oyarzun-Ampuero, Brea, Loza, Torres, & Alonso, 2009). The CS/CD nanoparticles with the advantages of good solubilization and permeability would improve the bioavailability of hydrophobic drugs. CDs have a hydrophobic central cavity and hydrophilic outer surface and can encapsulate substrates to form host guest complexes (Loftsson & Brewster, 1996; Szejtli, 1988; Uekama, Hirayama, & Irie, 1998). This complexation process normally results in a modulation of the properties of the guest molecule (*i.e.* the drug), such as increasing solubility, improving chemical and physical stability and enhancing absorption. Besides these capabilities, some studies have discussed their ability to optimize systemic dermal delivery through enhancement of drug release and/or permeation and sustaining drug release from vehicle (Matsuda & Arima, 1999). Due to its price, availability and cavity dimension, the β-CD is the most widely used.

The most popular approach for the formation of CD/hydrophilic polymer nanoparticles consists of the incorporation of a previously formed drug–CD inclusion complex into polymeric nanoparticles. In these systems, the presence of CDs generally results in an increased loading capacity for lipophilic drugs (Ceschel et al., 2003).

WAF is the most widely prescribed anticoagulant drug in North America (Holbrook et al., 2005). However, problems associated with oral WAF makes clear the continuing need for a new promising

* Corresponding author. Tel.: +20 1005406479; fax: +20 233370931.
E-mail addresses: safaakhk@yahoo.com (S.K.H. Khalil), gelfeky@hotmail.com (G.S. El-Feky), sallyelbanna77@yahoo.com (S.T. El-Banna), profwafaa_khalil@yahoo.com (W.A. Khalil).

0144-8617/$ – see front matter © 2012 Elsevier Ltd. All rights reserved.
http://dx.doi.org/10.1016/j.carbpol.2012.06.056

technology for its delivery in order to overcome the inconvenience of WAF therapy related to the variable effects resulting either from the high inter- and intra-individual variability in dose response due to its narrow therapeutic index or from its extensive interactions with food and medications and the related requirement for coagulation monitoring. Also, being a hydrophobic drug, WAF is practically insoluble in water and presents a very slow dissolution rate in acidic media.

Transdermal delivery avoids many problems associated with the oral route including drastic pH changes, the presence of enzymes, variable transit times and fluctuating drug plasma concentrations. In addition, it offers longer duration of action resulting in a reduction in dosing frequency, improved bioavailability, uniform plasma levels, reduced side effects as well as flexibility of terminating the drug administration by simply removing the patch from the skin (Bayarski, 2005). For transdermal therapy, the key point of dosage design is to enhance the drug solubility in the vehicle and improve its permeability *via* skin without causing irritation. Thus, our approach is to combine the benefits of CS as a penetration enhancing, biocompatible and rate controlling polymer of the nanoparticle generation together with those of CD as a solubility enhancer having the capability of bettering the solubility and stability of hydrophobic drugs like warfarin. Thus allowing their efficient encapsulation into hydrophilic carriers like chitosan nanoparticles to provide enhanced transdermal delivery of WAF capable of offering effective, non-toxic and controlled anti-coagulation.

2. Materials and methods

2.1. Materials

CS was purchased from Mallinckrodt, USA [M.W = 400,000, degree of deacetylation 95%]. Tripolyphosphate was supplied by Mallinckrodt, The Netherland. Glacial acetic acid 99.8% was obtained from El Nasr Pharmaceutical Chemicals Co., Egypt. WAF was purchased from Sigma–Aldrich, USA. Pharmaceutical grade β-CD was supplied by Roquette, France. Other chemicals and solvents were of analytical grade.

2.2. Preparation of WAF-β-CD complex

2.2.1. Phase solubility studies

Solubility study was carried out according to the method of Higuchi and Connors (1965). An excess drug (WAF) was added to distilled water containing different concentrations of β-CD. The formed suspensions were shaken at 25 ± 0.5 °C till equilibrium and then filtered through a millipore filter (0.45 μm). An aliquot portion of the filtrate was analyzed by UV spectrophotometer (UV-240 1PC, Shimadzu, Japan) at λ_{max} = 307 nm against blank. Experiment was performed in triplicate. The apparent stability constant ($K_{1:1}$) was calculated from the linear fit of the curve according to the following equation:

$$K_{1:1} = \frac{\text{slope}}{D_0(1 - \text{slope})}$$

where slope is the value found in the linear regression and D_0 is the intrinsic drug solubility derived from the intercept of the phase solubility relationship (Marcus, Brewster, & Loftsson, 2007).

2.2.2. WAF-β-CD complexation

Binary mixtures were prepared in a 1:1 molar ratio of WAF:β-CD based on the results obtained from the phase solubility study.

Physical mixture was prepared by simple mixing of the drug and the β-CD in a mortar for 10 min. *Kneaded complex* was obtained by adding small amount of water to WAF-β-CD mixture placed in a mortar until a homogeneous paste was obtained. The resulting paste was dried in an oven at 45 °C for 48 h and the solid was finally ground and sieved through a 250 μm sieve. *Co-evaporated complex* was obtained by dissolving equimolar amounts of β-CD and WAF in 250 ml of 50% aqueous ethanol. The solution was stirred up to complete dissolution of the powders; the solvent was then removed at reduced pressure using a rotary evaporator at 45 °C. The obtained solid was ground, sieved through a 250 μm sieve and placed in an oven at 45 °C for 48 h.

2.2.3. Characterization

2.2.3.1. Scanning electron microscopy (SEM). Complexes were gold coated using a Hitachi coating unit IB-2 coater under a high vacuum, 0.1 Torr, high voltage, 1.2 kV and 50 mA. Coated samples were examined using SEM (JEOL JXA-840A SEM, Japan) to characterize the changes of the drug surface before and after complexation for indicating complexation.

2.2.3.2. Fourier-transform infrared (FTIR) spectroscopy. FTIR spectra of the complexes were obtained on a 6100 JASCO FTIR spectrometer, Japan. A 1% of each dried complex was mixed with KBr and compressed to form tablets. The IR spectra were scanned over the wave number range of 4000–400 cm^{-1} using a resolution of 4 cm^{-1} and 64 co-added scans.

2.2.4. Analysis of drug content in the binary mixtures

Drug content was assayed by dissolving weighed amounts of each binary mixture in 10 ml of ethyl alcohol. The drug content was determined spectrophotometrically at 307 nm.

2.3. Preparation and characterization of blank CS nanoparticles

2.3.1. Preparation

CS nanoparticles preparation was based on the ionic gelation of CS with TPP anions (Calvo, Remunan-Lopez, Vila-Jato, & Alonso, 1997). CS nanoparticles were prepared in 2 groups, the first used different ratios of CS:TPP (1:1, 2:1, 3:1, 4:1, 5:1 and 6:1) with final CS concentration of 2 mg/ml. The second used different concentrations of CS (0.5, 1.0, 1.5, 2.0, 2.5 and 3.0 mg/ml) within the 3:1 CS:TPP ratio. In both groups, CS was first dissolved in acetic acid aqueous solution. The concentration of acetic acid in the aqueous media was 1.75 times that of CS. TPP aqueous solution was then added drop wise under magnetic stirring onto the corresponding amount of the CS solution at room temperature; 25 ± 1 °C.

2.3.2. Characterization

2.3.2.1. FTIR spectroscopy. See Section 2.2.3.2.

2.3.2.2. Transmission electron microscopy (TEM). TEM was used to determine the size and morphology of prepared nanopaticles. One drop of the nanoparticle colloidal suspension was spread onto a carbon film 200 mesh copper grid and allowed to stand for 10 min. The samples were stained with one drop of 3% phosphotungestic acid before viewing under microscope (JEOL JEM-1230, Japan).

2.4. Loading WAF-β-CD complex into CS nanoparticles

To load WAF into CS nanoparticles, the pH of the CS solution was adjusted to 5.4 using 0.1 N NaOH and a weighed amount of WAF-β-CD complex was then dissolved under magnetic stirring at room temperature. After the complete dissolution of WAF complex in the media, tripolyphosphate solution was added dropwise to the WAF-β-CD/CS solution. The mixture was stirred then sonicated.

2.4.1. Yield and entrapment efficiency CS nanoparticles

The yield of nanoparticles fabrication process was calculated by weighing dried samples of the isolated nanoparticles and referring them to the initial amounts of CS, tripolyphosphate and CD (Adlin, Nesalin, Gowthamarajan, & Somashekhara, 2009). The yield was calculated as follows:

$$\text{yeild} = \frac{\text{weight of nanoparticles}}{\text{total amount of the components}} \times 100$$

The nanoparticles were separated from the aqueous dispersion medium by centrifugation at 9000 rpm for 1 h. Entrapment efficiency (EE) was calculated based on the ratio of the amount of drug present in the nanoparticles to the initial amount of drug used in the loading process (Anitha et al., 2011).

$$EE(\%) = \frac{\text{total amount of drug in the nanoparticles}}{\text{initial amount of drug taken for loading studies}} \times 100$$

2.4.2. Preparation of nanoparticle powder

Dry powder of WAF-β-CD loaded CS nanoparticle was obtained by spray-drying the aqueous suspension of the nanoparticles using a laboratory-scale spray-dryer (Büchi® Mini Spray Dryer, B-290, Switzerland), under the following conditions; a feed rate of 2.5 ml/min, inlet and outlet temperatures of 120 ± 2 °C and 85 ± 2 °C, respectively, an air flow rate and aspirator kept constant at 400 Nl/h and 80%, respectively. Nanoparticles were collected and stored in a dessicator at room temperature until use (Grenha, Remunan-Lopez, Carvalho, & Seijo, 2008).

2.4.3. Characterization of WAF-β-CD loaded CS nanoparticles

2.4.3.1. FTIR spectroscopy. See Section 2.2.3.2.

2.4.3.2. TEM. See Section 2.4.2.

2.4.3.3. X-ray diffraction (XRD). The XRD experiments were carried out using X-ray diffractometer (Empyrean, Pixcel^{3D}, Holland). Diffraction patterns of kneaded WAF-β-CD complex, blank CS NP and WAF-β-CD loaded CS NP were obtained at room temperature with powder diffractometer using a Cu Kα radiation (λ = 1.54060 Å), a current of 30 mA and voltage of 45 kV to study their chemical structures. Fine powdered samples, were analyzed over the 5–80 2θ range with a scan step size of 0.0260 and time of acquisition of 18.8700 s.

2.4.3.4. Zeta potential. The zeta potential of nanoparticles was measured using a Laser Zetameter (Malvern Instruments model "Zetasizer 2000", UK). Freshly prepared particles' suspension (0.01 g) was placed in 50 ml double distilled water at ionic strength of 2×10^{-2} M NaCl. The pH was adjusted to the required value. The sample was shaken for 30 min. After shaking, equilibrium pH was recorded and zeta potential of the particles measured.

2.5. In vitro release of WAF from the prepared nanoparticles

Release of WAF from its β-CD complex alone as well as from the CS loaded WAF-β-CD complex nanoparticles was compared at 32 ± 0.5 °C using USP Dissolution Tester, Apparatus II, filled with 900 ml phosphate buffer of pH 5.5 at a rotation rate of 50 rpm. In addition drug release from CS loaded WAF-β-CD complex nanoparticles was compared at pH 5.5 and 7.4. Aliquots, each of 5 ml, were withdrawn at different time intervals up to 8 h and replenished by equal volumes of fresh dissolution medium. WAF content was measured spectrophotometrically at 307 nm. The percentage drug released and release profile were evaluated.

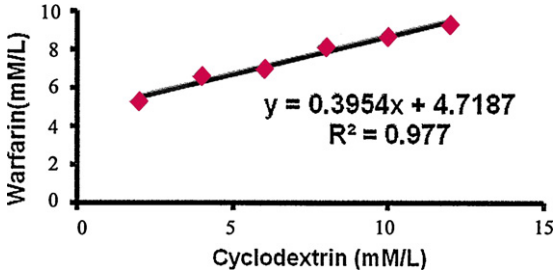

Fig. 1. Effect of β-cyclodextrins on the solubility of warfarin.

2.6. Ex vivo WAF permeation of the prepared nanoparticles

The permeation of WAF through excised rat skin was carried out using Franz diffusion cells. The receptor compartment was filled with phosphate buffer, pH 7.4, stirred continuously using a magnetic stirrer. The temperature of the receptor compartment was kept at 37 °C. The skin was mounted between the donor and receptor compartments of the Franz diffusion cell. The prepared formula was placed in the donor compartment. At predetermined time intervals, samples were taken from the receptor compartment and the cell refilled with an equivalent amount of fresh buffer solution.

3. Results and discussion

3.1. WAF-β-CD complex formation

3.1.1. Phase solubility study

The apparent solubility of WAF increased linearly as a function of β-CD concentration over the studied concentration range (Fig. 1) which is a characteristic of A_L-type system (Higuchi & Connors, 1965). The slope value was lower than one indicating an inclusion complex in the molar ratio of 1:1 between the guest (WAF) and host (β-CD) molecules (Arima et al., 2001; Zingone & Rubessa, 2005). The solubilizing power of β-CD towards WAF was found to be 1.39×10^{-3} mM and the apparent stability constant, $K_{1:1}$, obtained from the slope of linear phase solubility diagram was found to be 138.59 M^{-1}. Large $K_{1:1}$ value suggests that the CD cavity is large which in turn favors the inclusion of WAF (Lin & Yang, 1986).

3.1.2. Characterization of WAF-β-CD complex

3.1.2.1. SEM. SEM demonstrated β-CD as parallelogram like structures having smooth surface with some irregularities (Fig. 2a) and WAF as apparent large rods with different sizes (Fig. 2b). WAF-β-CD physical mixture appeared as irregular rods of WAF adhered on the crystal surfaces of β-CD (Fig. 2c). The kneaded complex appeared as agglomerates clumping to each other (Fig. 2d), whereas the co-evaporation complex showed a new homogeneous interlocked crystal mass (Fig. 2e). These drastic changes reported with the kneaded and co-evaporated complexes indicate complete complex formation where the presence of a new single solid phase could be simply a consequence of a crystalline pattern change in these systems due to WAF-β-CD complex formation (Fernandes, Viera, & Veiga, 2002).

3.1.2.2. FTIR spectroscopy. The absorbance peak of WAF at 1074 cm^{-1} (C—O) was observed in the physical mixture but in the kneaded and co-evaporated mixtures it was slightly shifted to 1079 cm^{-1}. This was considered an indication of complex formation. The solid form of WAF has an IR absorption band at 998 cm^{-1} associated with the hemiketal ring (Stella, Mooney, & Pipkin, 1984). This peak was found in the physical mixture at 995 cm^{-1} and disappeared when inclusion complexes were formed by kneading and co-evaporation techniques (Fig. 3). This implies that when WAF

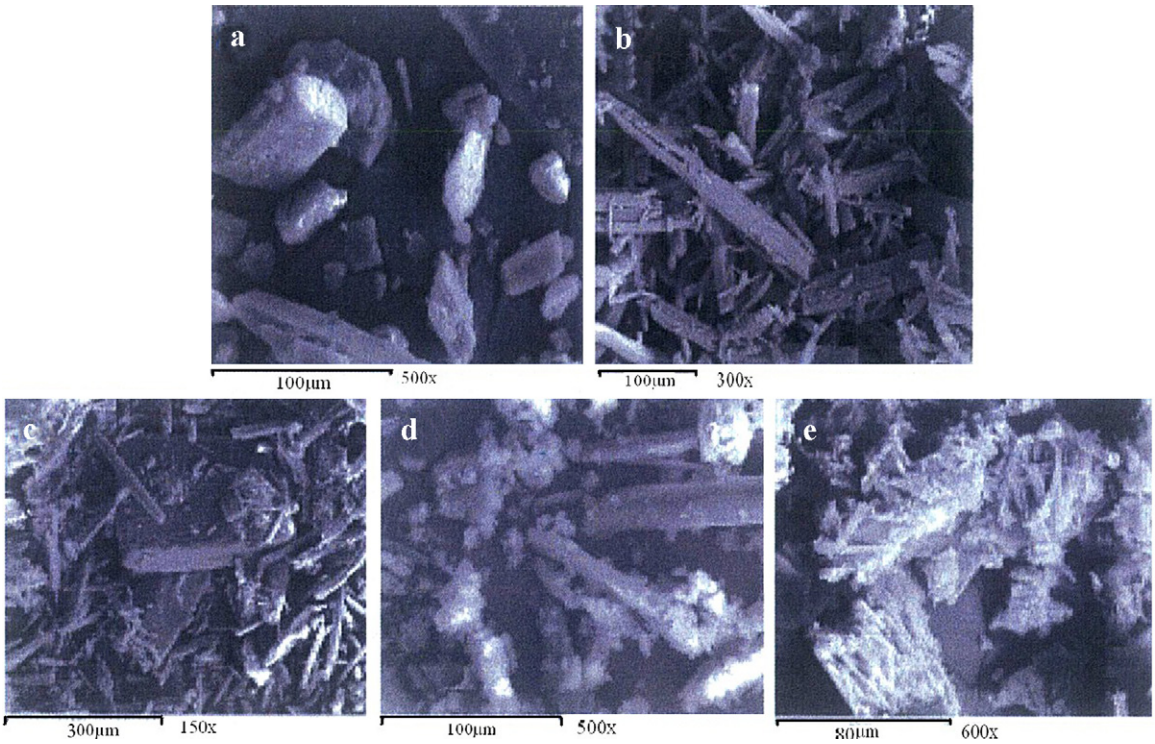

Fig. 2. SEM micrographs of (a) β-CD, (b) WAF, (c) WAF-β-CD physical mixture, (d) WAF-β-CD kneaded mixture and (e) WAF-β-CD co-evaporated mixture.

was included into the cavity of CD, it was changed from cyclic diastereometric hemiketal tautomer to open-chained tautomer in the solid complex state. These results are in good agreement with those previously reported (Lin & Yang, 1986).

3.1.2.3. WAF content in the drug–CD binary mixtures. Physical and kneaded mixtures showed a good agreement between theoretical and actual drug content (23 mg *vs.* 25 mg and 23 mg *vs.* 17.12 mg, respectively), whereas, in co-evaporated mixtures the actual drug content was much lower than that of the theoretical (23 mg *vs.* 3.96 mg). Based on this finding together with those obtained from SEM and FTIR, the kneading method was used for preparing drug–CD binary mixture.

3.2. Preparation and characterization of blank CS nanoparticles

Formation of chitosan nanoparticles depends on the ionic interaction between the positively charged CS and the polyanion TPP and the ability of CS to form a gel through inter- and intra-molecular linkages (Calvo et al., 1997).

3.2.1. FTIR spectroscopy

FT-IR spectroscopy was adopted to characterize the molecular structure of CS before and after nanoparticle formation. Careful investigation of the spectra of the CS nanoparticle in comparison to that of the pure CS revealed the following; the amino group (C=O amide I) absorption at 1646 cm^{-1} was shifted to 1644 cm^{-1} at the

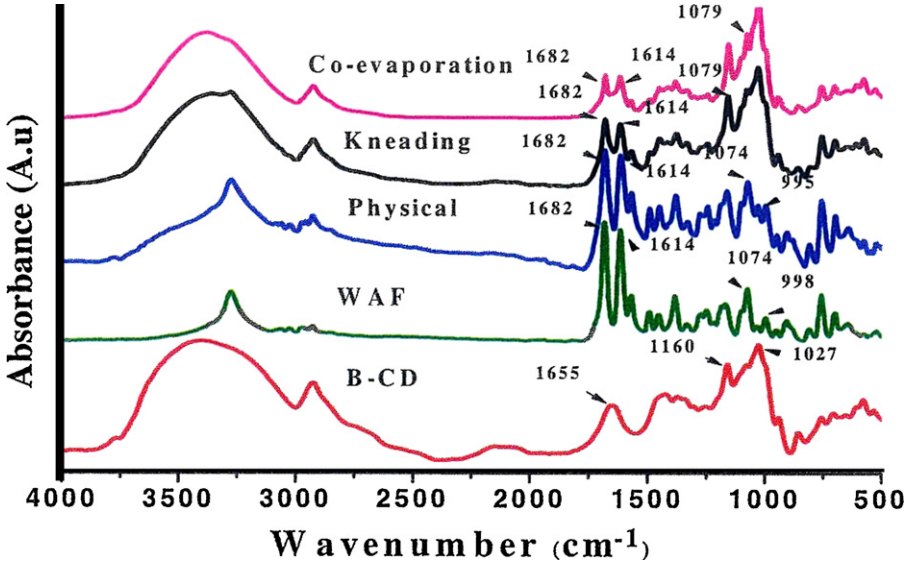

Fig. 3. FT-IR spectra of WAF, β-CD, WAF-β-CD physical, kneaded and co-evaporated complexes.

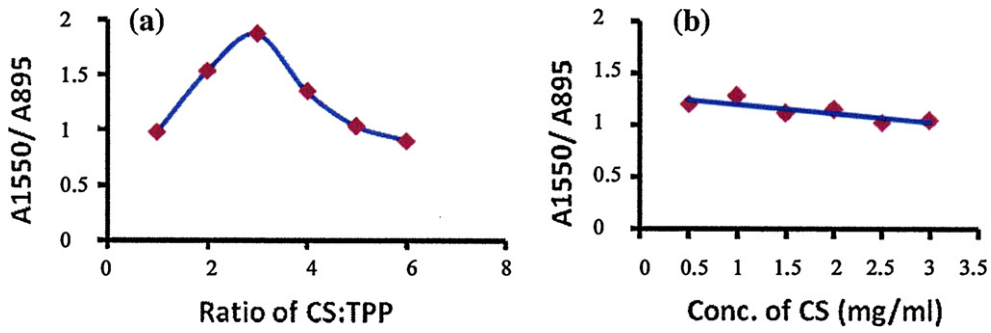

Fig. 4. The relationship between the absorbance ratio A 1550/A 895 with the different CS:TPP ratios (a) and different CS concentration (b).

CS:TPP ratios 1:1 and 2:1, and was shifted to 1640 cm^{-1} at the ratio 3:1. The CS:TPP ratios 4:1, 5:1 and 6:1 produced shifting of the amino group (amide I) absorption to 1635 cm^{-1}. The absorption peak at 1596 cm^{-1} specific to the amino groups (N—H amide II) of CS with high deacetylation degree, disappeared completely in the spectra of the CS:TPP ratios 1:1, 2:1 and 3:1 and a new absorption peak appeared at 1550 cm^{-1} as a result of nanoparticle formation with a gradually increased intensity from ratios 1:1 up to 3:1. For the ratios 4:1, 5:1 and 6:1, the spectra showed both; the peaks of the pure CS (1646 and 1596 cm^{-1}) and the new characteristic peak of the formed nanoparticles (1550 cm^{-1}). In order to quantify the CS nanoparticles formation along the studied CS:TPP ratios, the absorbance ratio (A 1550/A 895) was calculated using manual 2-point baseline method. The absorption peak at 1550 cm^{-1} was taken as a measure of the newly formed CS nanoparticle. The absorption peak at 895 cm^{-1} assigned to C—H stretching vibration of saccharine structure was taken as a reference band. The absorbance ratio was plotted against the different CS:TPP ratios (Fig. 4a). It is obvious that CS nanoparticle formation increased by increasing the CS:TPP ratio reaching a maximum value with CS:TPP weight ratio 3:1, this was followed by a gradual decline through the 4:1 and 5:1 ratios hitting its minimal value with the 6:1 ratio. This might be attributed to the insufficiency in the number of TPP molecules required to bond with the CS molecules with increasing CS concentration more than triple TPP concentration. Also, increasing the CS concentration could lower the free space available for the molecules to collide therefore decreasing the amount of ionizing bonds and subsequently the amount of nanoparticles formed. Thus, the 3:1 CS:TPP weight ratio was found ideal for nanoparticle formation; this comes in agreement with previous studies (Calvo et al., 1997; Zhang, Oh, Allen, & Kumacheva, 2004).

FT-IR spectra was then performed for pure CS and CS nanoparticles prepared with different CS concentrations (from 0.5 up to 3 mg/ml final CS concentration) within the CS:TPP weight ratio of 3:1. The amide I band 1646 cm^{-1} was shifted to 1640 cm^{-1} (0.5 mg/ml), 1644 cm^{-1} (1–2.5 mg/ml) and 1642 cm^{-1} (3 mg/ml). Furthermore, the absorption band at 1596 cm^{-1} in all CS concentrations (0.5, 1, 1.5, 2, 2.5 and 3 mg/ml) disappeared and new bands were formed at (1553, 1549, 1550, 1550, 1549 and 1547 cm^{-1}), respectively. FTIR results indicated that the amino group in all studied ratios and concentrations interacted with TPP creating ionic bonds. These interactions reduced CS solubility and were responsible for CS separation from solution in the form of nanoparticles. Furthermore, the new absorption band at 1550 cm^{-1} which appeared after the conjugation reaction with TPP, indicated the formation of new amide bonds through ionic interaction with TPP (Papadimitriou, Bikiaris, Avgoustakis, Karavas, & Georgarakis, 2008). Also, results showed that the CS:TPP ratio not the CS concentration is what plays the important role in determining the amount of nanoparticles formed where there was no obvious relationship between the concentration of CS and the amount CS nanoparticles formed (Fig. 4b), since the absorbance ratio (A 1550/A 895) appeared more or less constant with increasing CS concentration.

Table 1
Diameter of chitosan nanoparticles prepared by different ratios of CS:TPP and different concentrations of chitosan within the CS:TPP weight ratio of 3:1.

CS concentrations (mg/ml)	Mean diameter (*D* in nm)	S.D.	PDI
0.5	72	21.0	0.291
1.0	130	30.0	0.230
1.5	77	39.0	0.506
2.0	35	12.7	0.364
2.5	405	142.0	0.350
3.0	596	65.7	0.110

CS:TPP ratios	Mean diameter (*D* in nm)	S.D.	PDI
1:1	13	2.7	0.207
2:1	30	8.4	0.280
3:1	35	12.7	0.364
4:1	32	11.0	0.343
5:1	19	3.6	0.189
6:1	13	2.0	0.153

Notes: *D* is the mean value of at least 40 particles, S.D. is the standard deviation and PDI is the polydispersity index.

3.2.2. TEM

The ratio between CS and TPP is critical and controls the size and distribution of the nanoparticles and might in turn affect the biological performance of CS nanoparticles (Pan et al., 2002). Therefore, the effect of different CS:TPP weight ratios (1:1, 2:1, 3:1, 4:1, 5:1 and 6:1) on the size characteristics of prepared nanoparticles was studied. Results are represented in Fig. 5.1a–f. It could be observed that nanoparticles formed with ratios 1:1, 2:1, 4:1, 5:1 and 6:1 are roughly spherical and agglomerated while those formed with the ratio 3:1 (Fig. 5.1c) are separate and distinctly spherical. Table 1 shows that the particle size increased from 13 nm to 35 nm with increasing CS:TPP weight ratio from 1:1 up to 3:1, respectively, this was followed by a gradual decrease with further increasing CS:TPP weight ratio up to 6:1. It could be assumed that the decrease in the particle size at higher CS:TPP ratios is correlated with the reduction in the ionic bond formation (Calvo et al., 1997) indicating that the ideal particle size results when the availability of the functional groups on the two interacting polymers is in stoichiometric proportion. This contradicts the findings of Papadimitriou et al. (2008).

The effect of changing CS final concentrations (0.5, 1, 1.5, 2, 2.5 and 3 mg/ml); within the 3:1 CS:TPP weight ratio; on the particle size of the produced nanoparticles, was then investigated. The TEM micrographs of the formed nanoparticles showed distinct homogenous spherical morphology (Fig. 5.2a–f). Table 1 shows that the particle size was independent on the CS concentration up to

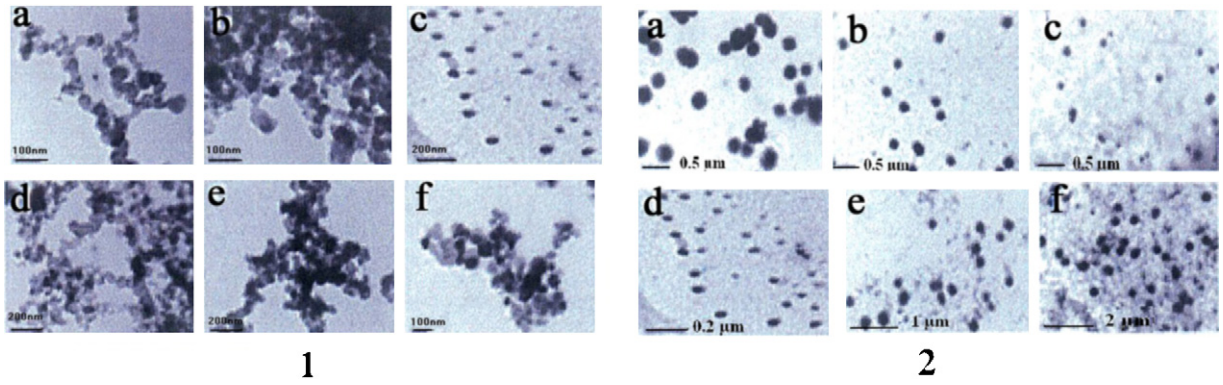

Fig. 5. TEM micrographs of CS nanoparticles prepared by different CS:TPP weight ratios (5.1); (a) 1:1, (b) 2:1, (c) 3:1, (d) 4:1, (e) 5:1 and (f) 6:1 and those prepared by different concentration of CS within the 3:1 CS:TPP weight ratio (5.2); (a) o.5 mg/ml, (b) 1 mg/ml, (c) 1.5 mg/ml, (d) 2 mg/ml, (e) 2.5 mg/ml and (f) 3 mg/ml.

2 mg/ml final CS concentration however, a remarkable increase in the particle size was reported with the 2.5 and 3.0 mg/ml final CS concentration (405 and 596 nm, respectively). This could be attributed to the increased possibility of each TPP molecule bonding to five CS molecules; through its five Na^+; with increasing the concentration of CS per unit volume. This might be the cause behind the formation of large sized particles. TEM results could be correlated to those of the quantitative FT-IR analysis (Fig. 4a and b).

3.3. WAF-β-CD loaded CS nanoparticles

3.3.1. Loading WAF-β-CD complex into CS nanoparticles

WAF-loaded CS nanoparticles were prepared in a two step procedure. The WAF-β-CD inclusion complex was prepared first (as previously described) then the complex was entrapped into the CS nanoparticles possessing the highest entrapment efficiency *via* the cross linking method.

3.3.2. Yield and entrapment efficiency of CS nanoparticles

The yield of all studied WAF loaded CS nanoparticles ranged from 62 to 88%. High nanoparticle recovery is favorable for reducing manufacturing costs (Douglas, Davis, & Lllum, 1987; Poovi, Lekshmi, Narayanan, & Reddy, 2011).

The entrapment efficiency (EE%) of nanoparticles, generally, depends on many factors, such as CS molecular weight, TPP content and CS concentration (Deng, Zhou, & Luo, 2006). The EE% of CS nanoparticles was found to increase from 73% to 94% with increasing the CS:TPP weight ratio from 1:1 up to 3:1, respectively. Further increase in the CS:TPP weight ratio did not result in any significant changes in drug entrapment. Hence, a series of increasing CS concentrations (0.5–3 mg/ml final CS concentration) within the weight ratio 3:1 was prepared and their entrapment efficiencies were determined.

A gradual increase in the entrapment efficiency was observed along the studied range of concentrations up to 2 mg/ml final CS concentration (from 30% up to 94% with 0.5 up to 2 mg/ml final CS concentration, respectively). Further increase in CS concentration led to a significant decrease in the entrapment of WAF reaching 24% with 3 mg/ml final CS concentration. It has been previously reported that the gradual and low increase in the viscosity of CS at lower concentrations (1–2 mg/ml) promotes the entrapment of WAF and gelation between CS and TPP (Wu, Yang, Wang, Hu, & Fu, 2005), until a certain limit above which the viscosity of the gelation medium highly increases with subsequent hindrance of drug entrapment (Kumar, Dharmendra, Jhansee, Shrikant, & Pandey, 2011; Vandenberg, Drolet, Scott, & Nöue, 2001; Wu et al., 2005).

The general trend of efficient entrapment reaching 94% of the hydrophobic drug into the hydrophilic CS nanoparticles could be mainly attributed to the primarily inclusion of the drug into the β-CD cavity which resulted in larger amounts of WAF available for association with CS nanoparticles.

Results of FT-IR, TEM and EE% demonstrated that the 3:1 CS:TPP ratio with 2 mg/ml final CS concentration offered the optimum conditions in the production of homogenous distinct smooth spherical CS nanoparticles (35 nm) with narrow particle size distribution range (PDI = 0.364). This finding coincides with that reported by Zhang in 2004 where he stated that, the CS:TPP (3:1) ratio lead to the most efficient cross-linkage of amino groups producing the most compact particle structure (Zhang et al., 2004). Therefore, drug-loaded nanoparticle formulation prepared at these conditions was adopted for intensive characterization using TEM, FT-IR, zeta-potential, *in vitro* release and *ex vivo* permeation.

3.3.3. Characterization of selected WAF-β-CD complex loaded CS nanoparticle

3.3.3.1. TEM. Using TEM, WAF complex loaded CS nanoparticles appeared as distinct, spherical and regular (Fig. 6a) with a mean particle size diameter of 63 ± 23 nm and a relatively narrow particle size distribution (PDI = 0.368). It is noted that, the incorporation of WAF into CS nanoparticles led to an increase in their size compared to the blank nanoparticles (Chen, Mohanraj, & Parkin, 2003; Kim et al., 2006; Papadimitriou et al., 2008).

3.3.3.2. FT-IR. FT-IR spectra of WAF, blank CS nanoparticles and WAF-β-CD complex loaded CS nanoparticles revealed spectral changes resulting from WAF encapsulation (Fig. 6b). The C=O amid I peak at 1644 cm^{-1} of the blank CS nanoparticle was shifted to 1646 cm^{-1} and its intensity decreased markedly changing into a shoulder. The new absorption peak at 1550 cm^{-1} (due to nanoparticles formation) was shifted to 1571 cm^{-1} after drug loading. The major characteristic peaks of warfain; 1682 cm^{-1} (C=O) and 1614 cm^{-1} (C=C aromatic ring) disappeared while 1074 cm^{-1} (C—O) remained. FT-IR changes indicated the strong interaction developed between the C=O group of WAF and the NH_2 group of CS/TPP matrix with drug loading (Anitha et al., 2011; Chen et al., 2003; Papadimitriou et al., 2008).

3.3.3.3. XRD. Blank CS NP diffraction pattern showed some major peaks at approximately 11°, 19°, 22.5°, 29°, 44.5° and 72.5° with strongest intensity at $2\theta = 44.5°$. The kneaded WAF-β-CD binary mixture presented several peaks implying their crystalline nature. The diffraction pattern of WAF-β-CD loaded CS NP exhibited the characteristic peaks of the blank CS NP together with only one intense peak due to the drug–CD complex (at 9°), indicating that WAF may present as molecular dispersion in the polymeric nanoparticle (Jingou et al., 2011).

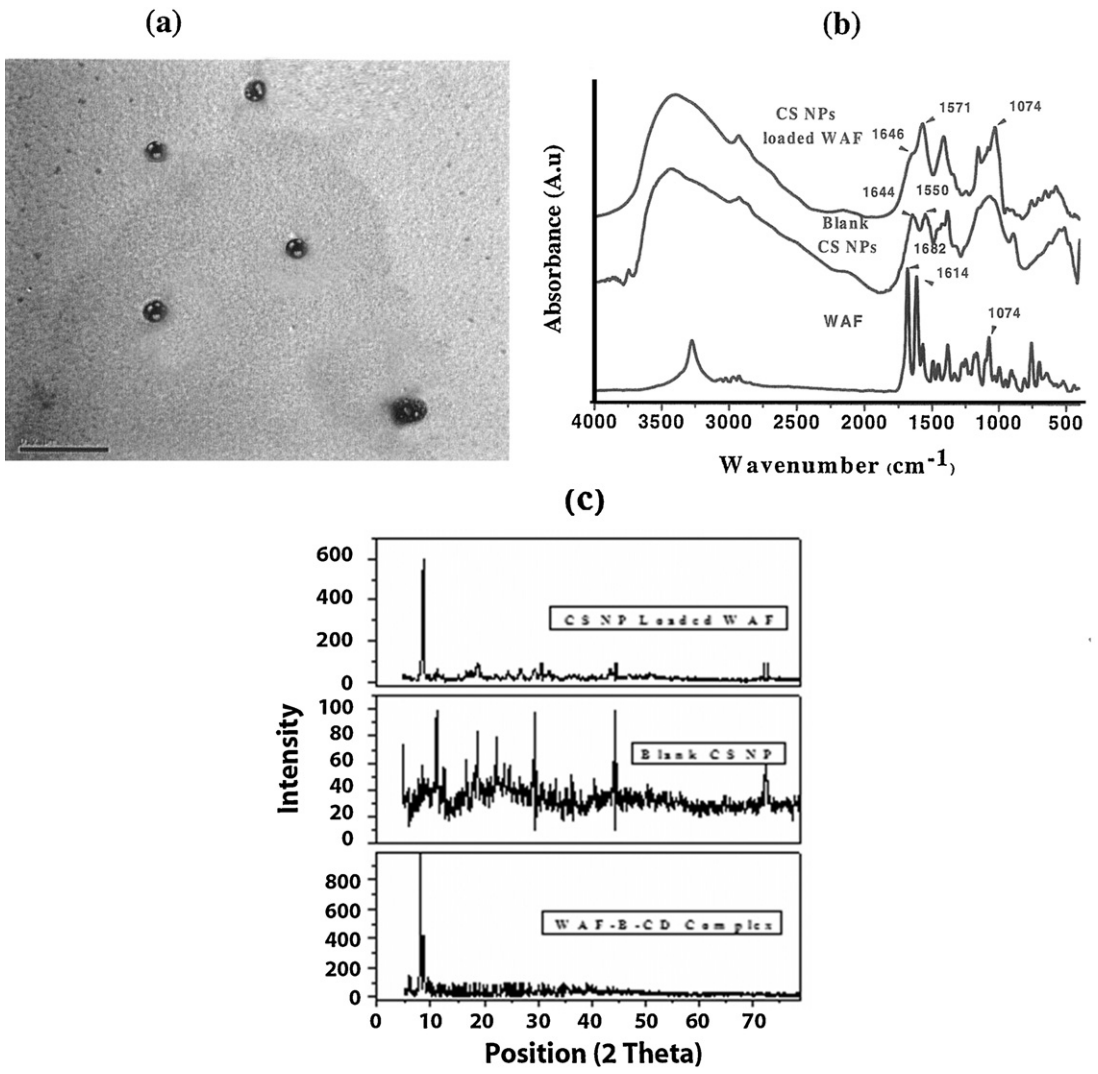

Fig. 6. Characteristics of warfarin-β-CD loaded chitosan nanoparticles, (a) TEM micrographs, (b) FT-IR spectra and (c) X-ray diffraction.

3.3.3.4. Zeta potential. The incorporation of WAF into CS nanoparticles had significant effect on the zeta potential values, where an increase in the mean particle size of the blank and drug loaded nanoparticles from 35 nm to 63 nm, respectively was accompanied by a decrease in the zeta potential value from 32.4 mV to 19.8 mV, respectively. Similar results were reported when heparin was incorporated into CS/γ-PGA nanoparticles (Tang et al., 2010) and when quercetin was incorporated into CS particles (Liu & Guo, 2006). Positive zeta potential values could be attributed to the residual amino groups of CS molecules entangled onto the surface of the nanoparticles (Oyarzun-Ampuero et al., 2009; Jingou et al., 2011). This positive charge is desirable in order to prevent particles aggregation and to promote electrostatic interaction with the overall negative charge of the cell membrane (Schillers et al., 2004).

3.3.3.5. In vitro release of WAF from the prepared nanoparticles. An important requirement of successful transdermal therapy is that a drug carried by a vehicle be able to reach the skin surface at an adequate rate and in sufficient amounts. This makes studying the release profile of WAF from nanoparticles crucial in order to predict the behavior of the drug during its transdermal delivery.

The release data were fitted to different kinetic equations and showed that WAF release from the CS nanoparticles followed a Higuchi release model. WAF release showed a very rapid initial burst that lasted for 2 h at which approximately 40–50% of the drug content was released from the nanoparticles this was followed by a slower and more gradual drug release pattern reaching approximately 65% at 8 h (Fig. 7a). In 2006, Maestrelli et al., reported a typical release profile characterized by an initial rapid release phase that reached a plateau in a relatively short time (1.5 h) due to an initially released drug–CD complex by simple diffusion through the CS network followed by drug release due to degradation of the polymeric matrix (Maestrelli, Garcia-Fuentes, Mura, & Alonso, 2006). This comes also in agreement with recent studies in drug loaded-CS nanoparticles (Boonsongrit, Mitrevej, & Mueller, 2006). The initial fast release might be the result of the dispersion of drug–CD molecules close to the nanoparticles surface, thus allowing easy diffusion in the initial incubation time through the porous surface of the nanoparticles. After the burst release period, the rate of release decreased as the dominate release mechanism might have changed to drug–CD complex diffusion through the CS matrix followed by drug exposure due to polymer erosion (Papadimitriou et al., 2008; Zhang, Wu, Tao, Zang, & Su, 2010).

The presence of CD within the drug loaded nanoparticle formulation could have contributed to the sustained release effect exhibited by the CS nanoparticles. In a recent study by Jingou et al., the release rate of calcium folinate (CaF) from the CS/CD nanoparticles was found to be higher and more sustained than methotrexate (MTX) from CS only nanoparticles (Jingou et al., 2011).

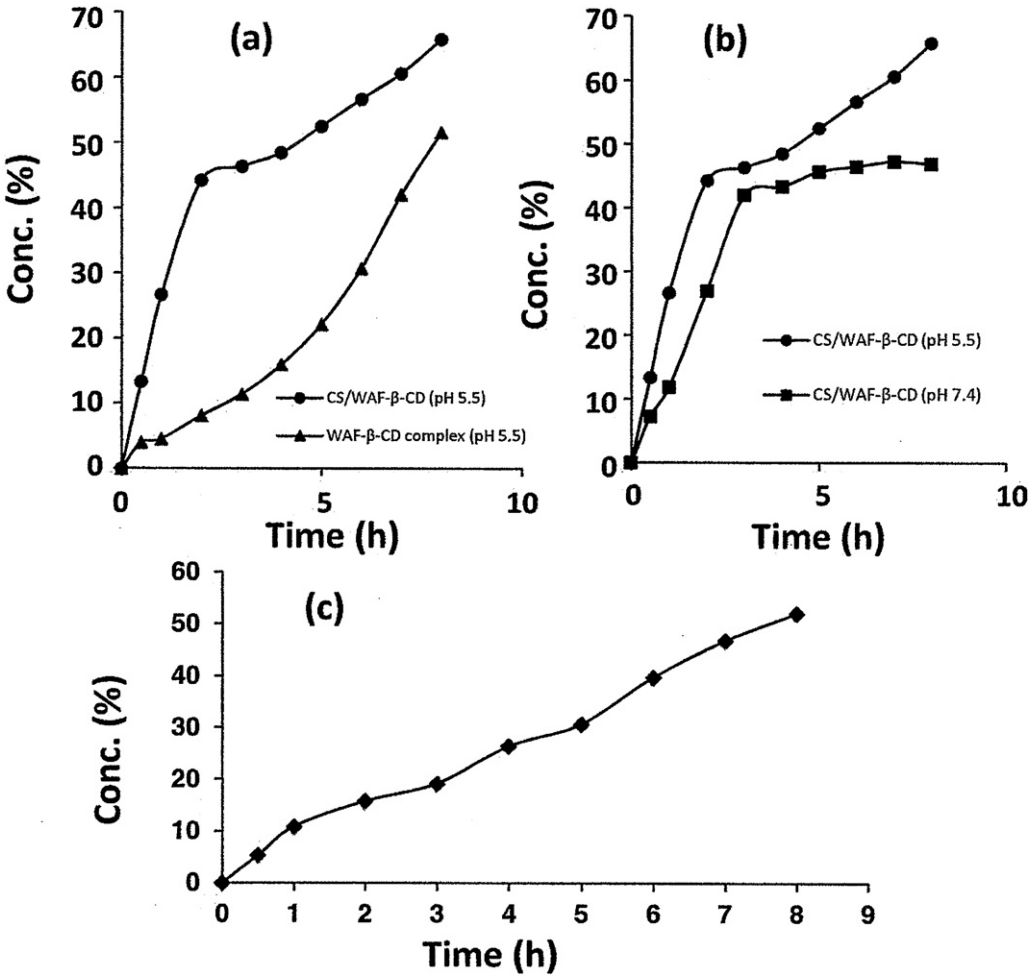

Fig. 7. *In vitro* drug release profile of warfarin-β-CD complex and warfarin-β-CD loaded chitosan nanoparticles at pH 5.5 (a) and pH 7.4 (b). *Ex vivo* drug permeation of warfarin-β-CD loaded chitosan nanoparticles at pH 7.4 (c).

Comparing the *in vitro* drug release profile from WAF-β-CD complex with that of WAF-β-CD loaded chitosan nanoparticles at pH 5.5 a different monophasic release pattern was observed, where, gradual slower zero order release profile was reported (R^2; 0.9456), total percentage drug released at 8 h was found to be 51.56% *i.e.* about 14% less than the total percentage released from CS loaded warfarin-β-CD complex (Fig. 7a). This could be attributed to what was previously reported by Zerrouk et al., in 2006 that the presence of CS strongly reduces the drug–Cd complex stability, thus increasing the amount of free drug released and in turn available for permeation (Zerrouk et al., 2006).

Furthermore, comparing the drug release profile from WAF-β-CD loaded CS nanoparticles at pH 5.5 and 7.4 (Fig. 7b), it was found that the drug release at pH 7.4 followed the same biphasic release pattern (initial burst followed by subsequent gradual release) as at pH 5.5, however, the release rate during both phases was lower and during an 8 h experiment, the amount drug released reached a total percentage of 46.87% compared to 65.78 at pH 5.5, this might be attributed to the reduced solubility of chitosan at pH above 6.8 (Wen, Xianxi, Lihai, & Feng, 2009). This finding supported by the hypothesis that chitosan carriers release drugs on the skin surface and binds covalently with the negatively charged stratum corneum increasing its fluidity and enhancing drug permeability (Taveira, Nomizo, & Lopez, 2009) goes with our selection of pH 5.5 as the most suitable media for assessing the release profile of the drug.

3.3.3.6. Ex vivo WAF permeation of the prepared nanoparticles. Ex vivo permeation experiments were carried out through excised rat skin. It was shown that permeation studies using rat skin is capable of providing information useful for manipulating the design of transdermal drug systems so that the desired permeation of the drug across human skin would be achieved (Al-Saidan, 2004).

As shown in (Fig. 7c), a steady increase in the amount of permeated drug in the receptor compartment with time was observed. It was found that WAF permeation through excised rat skin followed a typical zero order kinetics (R^2 = 0.991) with approximately 60% of the drug released after 8 h. This could be a result of CS nanoparticle acting as drug reservoir, where drug is released from the inner phase to the outer phase and then further into the skin (Peltola, Saarinen-Savolainen, Kiesvaara, & Suhonen, 2003). This reservoir effect makes depletion of WAF in the external phase due to its permeation into the skin constantly replenished by the release of WAF from the internal phase, thus leading to zero order permeation profile. The facilitated permeability of WAF from rat skin could be attributed to the favorable synergistic effect from the simultaneous presence of the two types of carriers; β-CD and CS where β-CD is known to act as a permeation enhancer in transdermal drug delivery (Krauland & Alonso, 2007) while, CS and its derivatives could significantly change the secondary structure of keratin in stratum corneum, increase the water content in stratum corneum, decrease HaCaT cell membrane potential and enhance cell membrane fluidity to various degrees.

Also, such results could be due to the marked decrease of the WAF–CD complex stability constant resulting from the presence of CS leading to an increase of the free drug amount available for permeation, and thus, rendering the enhancing effect of CD on WAF permeation evident (Zerrouk et al., 2006).

Release and permeation studies of WAF from CS nanoparticles indicated that the percentage drug released from the prepared nanoparticles correlates well with the percentage permeated (approximately 60% in 8 h) through the skin. This suggests that nanoparticles structures allow high drug mobility in the vehicle leading to faster drug diffusion to the skin surface, and thus, a higher transdermal delivery (Kreilgaard, 2002).

4. Conclusion

WAF-β-CD loaded CS nanoparticles were successfully prepared by ionic gelation method. CS nanoparticles were found to be spherical, smooth and with narrow size distribution. They showed high drug entrapment efficiency and well accepted yield. The release profile of WAF-β-CD complex from nanoparticles showed an initial burst effect followed by a slow and continuous release phase. The nanoparticle formulation enhanced the permeation of WAF through excised rat skin in a constant and continuous profile. Therefore, it could be concluded that combining the virtues of β-CD and CS was a good tool for enhancing its controlled release and successful permeation, thus, offering a promising system for the transdermal delivery of WAF.

References

Adlin, J., Nesalin, J., Gowthamarajan, K., & Somashekhara, C. N. (2009). Formulation and evaluation of nanoparticles containing flutamide. *International Journal of ChemTech Research*, *1*, 1331–1334.

Al-Saidan, S. M. (2004). Transdermal self-permeation enhancement of ibuprofen. *Journal of Controlled Release*, *100*, 199–209.

Anitha, A., Maya, S., Deepa, N., Chennazhi, K. P., Nair, S. V., & Tamura, H. (2011). Efficient water-soluble biodegradable polymeric nanocarrier for the delivery of curcumin to cancer cells. *Carbohydrate Polymers*, *83*, 452–461.

Arima, H., Yunomae, K., Miyake, K., Irie, T., Hirayama, F., & Uekama, K. (2001). Comparative studies of the enhancing effects of cyclodextrins on the solubility and oral bioavailability of tacrolimus in rats. *Journal of Pharmaceutical Sciences*, *90*, 690–701.

Bayarski, Y. Transdermal drug delivery, transdermal patches. (2005). Available from: http://ezinearticles.com/?Transdermal-Drug-Delivery,-Transdermal-Patches&id=155961.

Boonsongrit, Y., Mitrevej, A., & Mueller, B. W. (2006). Chitosan drug binding by ionic interaction. *European Journal of Pharmaceutics and Biopharmaceutics*, *62*, 267–274.

Calvo, P., Remunan-Lopez, C., Vila-Jato, J. L., & Alonso, M. J. (1997). Chitosan and chitosan/ethylene oxide–propylene oxide block copolymer nanoparticles as novel carriers for proteins and vaccines. *Pharmacal Research*, *14*, 1431–1436.

Ceschel, G., Bergamante, V., Maffei, P., Borgia Lambardi, S., Calabrese, V., Biserni, S., et al. (2003). Solubility and transdermal permeation properties of a dehydroepiandrosterone cyclodextrin complex from hydrophilic and lipophilic vehicles. *Drug Delivery*, *12*, 275–280.

Chen, Y., Mohanraj, V. J., & Parkin, J. E. (2003). Chitosan-dextran sulfate nanoparticles for delivery of an antiangiogenesis peptide. *International Journal of Peptide Research and Therapeutics*, *10*, 621–629.

De Campos, A. M., Sanchez, A., & Alonso, M. J. (2001). Chitosan nanoparticles: A new vehicle for the improvement of the delivery of drugs to the ocular surface application to cyclosporine. *International Journal of Pharmaceutics*, *224*, 159–168.

Deng, Q. Y., Zhou, C. R., & Luo, B. H. (2006). Preparation and characterization of chitosan nanoparticles containing lysozyme. *Pharmaceutical Biology*, *44*, 336–342.

Douglas, S. J., Davis, S. S., & Lllum, L. (1987). Nanoparticles in drug delivery. *CRC Critical Reviews in Therapeutic Drug Carrier Systems*, *3*, 233–261.

Fernandes, C., Viera, M. T., & Veiga, F. (2002). Physicochemical chraracterization and in vitro dissolution behavior of nicardipinecyclodextrins inclusion compounds. *European Journal of Pharmaceutical Sciences*, *15*, 79–88.

Grenha, A., Remunan-Lopez, C., Carvalho, E. L., & Seijo, B. (2008). Microspheres containing lipid/chitosan nanoparticles complexes for pulmonary delivery of therapeutic proteins. *European Journal of Pharmaceutics and Biopharmaceutics*, *69*, 83–93.

Higuchi, T., & Connors, K. A. (1965). Phase-solubility techniques. *Advances in Analytical Chemistry and Instrumentation*, *4*, 212–217.

Holbrook, A. M., Pereira, J. A., Labiris, R., McDonald, H., Douketis, J. D., Crowther, M., et al. (2005). Systematic overview of WARFARIN and its drug and food interactions. *Archives of Internal Medicine*, *165*, 1095–1106.

Illum, L., Jabbal-Gill, I., Hinchcliffe, M., Fisher, A. N., & Davis, S. S. (2001). Chitosan as a novel nasal delivery system for vaccines. *Advanced Drug Delivery Reviews*, *51*, 81–96.

Jingou, Ji, Shilei, H., Weiqi, L., Danjun, W., Tengfei, W., & Yi, Xu. (2011). Preparation, characterization of hydrophilic and hydrophobic drug in combine loaded chitosan/cyclodextrin nanoparticles and in vitro release study. *Colloids and Surfaces B: Biointerfaces*, *83*, 103–107.

Kim, D. G., Jeong, Y. I., Choi, C., Roh, S. H., Kang, S. K., Jang, M. K., et al. (2006). Retinol encapsulated low molecular water-soluble chitosan nanoparticles. *International Journal of Pharmaceutics*, *319*, 130–138.

Krauland, A. H., & Alonso, M. J. (2007). Chitosan/cyclodextrin nanoparticles as macromolecular drug delivery system. *International Journal of Pharmaceutics*, *340*, 134–142.

Kreilgaard, M. (2002). A ssessment of cutaneous drug delivery using microdialysis. *Advanced Drug Delivery Reviews*, *1*, 99–121.

Kumar, D. A., Dharmendra, S., Jhansee, M., Shrikant, N., & Pandey, S. P. (2011). Development and characterization of chitosan nanoparticles loaded with Amoxycilin. *International Research Journal of Pharmacy*, *2*, 145–151.

Langoth, N., Kahlbacher, H., Schöffmann, G., Schmerold, I., Schuh, M., Franz, S., et al. (2006). Thiolated chitosans: Design and in vivo evaluation of a mucoadhesive buccal peptide drug delivery system. *Pharmaceutical Research*, *23*, 573–579.

Lin, S. Y., & Yang, J. C. (1986). Inclusion complexation of WARFARIN with cyclodextrins to improve some pharmaceutical characteristics. *Pharmaceutisch Weekblad-Scientific Edition*, *8*, 223–228.

Liu, W., & Guo, Y. (2006). Interaction between flavonoid, quercetin and surfactant aggregates with different charges. *Journal of Colloid and Interface Science*, *302*, 625–632.

Loftsson, T., & Brewster, M. E. (1996). Pharmaceutical applications of cyclodextrins. I. Drug solubilization and stabilization. *Journal of Pharmaceutical Sciences*, *85*, 1017–1025.

Maestrelli, F., Garcia-Fuentes, M., Mura, P., & Alonso, M. J. (2006). A new drug nanocarrier consisting of chitosan and hydoxypropylcyclodextrin. *European Journal of Pharmaceutics and Biopharmaceutics*, *63*, 79–86.

Marcus, E., Brewster, M. E., & Loftsson, T. (2007). Cyclodextrins as pharmaceutical solubilizers. *Advanced Drug Delivery Reviews*, *59*, 645–666.

Matsuda, H., & Arima, H. (1999). Cyclodextrins in transdermal and rectal delivery. *Advanced Drug Delivery Reviews*, *36*, 81–99.

Mei, D., Mao, S., Sun, W., Wang, Y., & Kissel, T. (2008). Effect of chitosan structure properties and molecular weight on the intranasal absorption of tetramethylpyrazine phosphate in rats. *European Journal of Pharmaceutics and Biopharmaceutics*, *70*, 874–881.

Morishita, M., & Peppas, N. A. (2006). Is the oral route possible for peptide and protein drug delivery. *Drug Discovery Today*, *11*, 905–910.

Muzzrelli, R. A. A. (2012). Chemical and technological advances in chitins and chitosans useful for the formulation of biopharmaceuticals. In B. Sarmento, & DasNeves (Eds.), *Chitosan-based systems for biopharmaceuticals* (pp. 3–22). New York: Wiley.

Oyarzun-Ampuero, F. A., Brea, J., Loza, M. I., Torres, D., & Alonso, M. J. (2009). Chitosan-hyaluronic acid nanoparticles loaded with heparin for the treatment of asthma. *International Journal of Pharmaceutics*, *381*, 122–129.

Ozcan, I., Abaci, O., Uztan, A. H., Aksu, B., Boyacioğlu, H., Güneri, T., et al. (2009). Enhanced topical delivery of terbinafine hydrochloride with chitosan hydrogels. *AAPS Pharmaceutical Science and Technology*, *10*, 1024–1031.

Pan, Y., Li, Y. J., Zhao, H. Y., Zheng, J. M., Xu, H., Wei, G., et al. (2002). Bioadhesive polysaccharide in protein delivery system: Chitosan nanoparticles improve the intestinal absorption of insulin in vivo. *International Journal of Pharmaceutics*, *249*, 139–147.

Panyam, J., & Labhasetwar, V. (2003). Biodegradable nanoparticles for drug and gene delivery to cells and tissue. *Advanced Drug Delivery Reviews*, *55*, 329–347.

Papadimitriou, S., Bikiaris, D., Avgoustakis, K., Karavas, E., & Georgarakis, M. (2008). Chitosan nanoparticles loaded with dorzolamide and pramipexole. *Carbohydrate Polymers*, *73*, 44–54.

Peltola, S., Saarinen-Savolainen, P., Kiesvaara, J., & Suhonen, T. M. (2003). Microemulsions for topical delivery of estradiol. *International Journal of Pharmaceutics*, *254*, 99–107.

Poovi, G., Lekshmi, U. M. D., Narayanan, N., & Reddy, N. (2011). Prepration and characterization of repaglinide loaded chitosan polymeric nanoparticles. *Research Journal of Nanoscience and Nanotechnology*, *1*, 12–24.

Schillers, J., Naji, L., Trampel, R., Ngwa, W., Knauss, R., & Arnold, K. (2004). Pulsed-field gradient-nuclear magnetic resonance (PFG NMR) to measure the diffusion of ions and polymers in cartilage. In F. De Ceuninck, P. Pastoureau, & M. Sabatini (Eds.), *Osteoarthritis: Methods and protocols* (pp. 287–302). Totowa: Humana Press.

Shenoy, D. B., & Amiji, M. M. (2005). Poly (ethyleneoxide)-modified poly (epsilon caprolactone) nanoparticles for targeted delivery of tamoxifrnin breast cancer. *International Journal of Pharmaceutics*, *293*, 261–270.

Stella, V. J., Mooney, K. G., & Pipkin, J. D. (1984). Dissolution and ionization of WARFARIN. *Journal of Pharmaceutical Sciences*, *73*, 946–948.

Szejtli, J. (1988). Introduction and general overview of cyclodextrin chemistry. *Chemical Reviews*, *98*, 1743–1753.

Tang, D. W., Yu, S. H., Ho, Y. C., Mi, F. L., Kuo, P. L., & Sung, H. W. (2010). Heparinized chitosan/poly(g-glutamic acid) nanoparticles for multi-functional delivery of fibroblast growth factor and heparin. *Biomaterials*, *31*, 9320–9332.

Taveira, S. F., Nomizo, A., & Lopez, R. F. V. (2009). Effect of the iontophoresis of a chitosan gelon doxorubicin skin penetration and cytotoxicity. *Journal of Controlled Release*, *134*, 35–40.

Uekama, K., Hirayama, F., & Irie, T. (1998). Cyclodextrin drug carrier systems. *Chemical Reviews*, *98*, 2045–2076.

Vandenberg, G. W., Drolet, C., Scott, S. L., & Nöue, J. D. (2001). Factors affecting protein release from alginate-chitosan coacervate microcapsules during production and gastric/intestinal simulation. *Journal of Controlled Release*, *77*, 297–307.

Wen, H., Xianxi, G., Lihai, X., & Feng, M. (2009). Study on the mechanisms of chitosan and its derivatives used as transdermal penetration enhancers. *International Journal of Pharmaceutics*, *382*, 234–243.

Wilson, B., Sammanta, M. K., Santhi, K., Kumar, K. P., Ramasamy, M., & Suresh, B. (2009). Chitosan nanoparticles as a new delivery system for anti-Alzheimer's drug tacrine. *Nanomedicine*, *6*, 144–152.

Wu, Y., Yang, W., Wang, C., Hu, J., & Fu, S. (2005). Chitosan nanoparticles as a novel delivery system for ammonium glycyrrhizinate. *International Journal of Pharmaceutics*, *295*, 235–245.

Zerrouk, N., Courti, G., Ancillotti, S., Maestrelli, F., Cerri, M., & Mura, P. (2006). Influence of cyclodextrins and chitosan, separately or in combination, on glyburide solubility and permeability. *European Journal of Pharmaceutics and Biopharmaceutics*, *62*, 241–246.

Zhang, H., Oh, M., Allen, C., & Kumacheva, E. (2004). Monodisperese chitosan nanoparticles for mucosal drug delivery. *Biomacromolecules*, *5*, 2461–2468.

Zhang, H. L., Wu, S. H., Tao, Y., Zang, L. Q., & Su, Z. Q. (2010). Preparation and characterization of water-soluble chitosan nanoparticles as protein delivery system. *Journal of Nanomaterials*, *2010*, 5.

Zingone, G., & Rubessa, F. (2005). Preformulation study of the inclusion complex WARFARIN-β-cyclodextrin. *International Journal of Pharmaceutics*, *291*, 3–10.